Biosensors and Bioelectronics 38 (2012) 295–301

Contents lists available at SciVerse ScienceDirect

Biosensors and Bioelectronics

journal homepage: www.elsevier.com/locate/bios

# A novel glucose biosensor using bi-enzyme incorporated with peptide nanotubes

Byung-Wook Park [a], Rui Zheng [b], Kyoung-A Ko [c], Brent D. Cameron [b], Do-Young Yoon [d], Dong-Shik Kim [a,*]

[a] Department of Chemical and Environmental Engineering, University of Toledo, Toledo, OH 43606, United States
[b] Department of Bioengineering, University of Toledo, Toledo, OH 43606, United States
[c] Department of Pharmacology, University of Toledo, Toledo, OH 43606, United States
[d] Department of Chemical Engineering, Kwangwoon University, Seoul 139-701, Republic of Korea

ARTICLE INFO

*Article history:*
Received 29 February 2012
Received in revised form
4 June 2012
Accepted 4 June 2012
Available online 13 June 2012

*Keywords:*
Glucose biosensor
Bi-enzyme
Peptide nanotube (PNT)
Binary self-assembled monolayer (SAM)
Encapsulation
Amperometric sensor

ABSTRACT

A novel amperometric glucose biosensor was developed using the bio-inspired peptide nanotube (PNT) as an encapsulation template for enzymes. Horseradish peroxidase (HRP) was encapsulated by the PNT and glucose oxidase ($GO_x$) was co-immobilized with the PNT on a gold nanoparticle (AuNP)-modified electrode. A binary SAM of 3-mercaptopropionic acid (MPA) and 1-tetradecanethiol (TDT) was formed on the surface of the electrode to immobilize the PNT and $GO_x$. The resulting electrode appeared to provide the enzymes with a biocompatible nanoenvironment as it sustained the enhanced enzyme activity for an extended time and promoted possible direct electron transfer through the PNT to the electrode. Performance of the biosensor was evaluated in terms of its detection limit, sensitivity, pH, response time, selectivity, reproducibility, and stability in a lab setting. In addition the sensor was tested for real samples. The composite of AuNP-SAM-PNT/HRP-$GO_x$ to fabricate a sensor electrode in this study exhibited a linear response with glucose in the concentration range of $0.5-2.4$ mM with a $R^2$-value of 0.994. A maximum sensitivity of 0.3 mA $M^{-1}$and reproducibility (RSD) of 1.95% were demonstrated. The PNT-encapsulated enzyme showed its retention of $>85\%$ of the initial current response after one month of storage.



## 1. Introduction

The nanostructures built up of biomolecules have gained great attraction since they show electrochemical conductivity, versatility of chemical and biological modification, and biocompatibility. Possible fabrication of useful molecular conformation by bottom-up approaches is another advantage (Adler-Abramovich et al., 2010; Gazit, 2007; Reches and Gazit, 2006). Several biomolecules such as peptides, lipids, DNA, RNA and proteins can be self-assembled into highly ordered nanostructures. In particular, a peptide consisting of several to dozens of amino acids has been a class of versatile building blocks (Yan et al., 2010). Reches and Gazit introduced a peptide which consists of two phenylalanine residue (Phe–Phe) and they showed that it forms a self-assembled peptide nanotube (PNT). Since then, the nanostructure composed of dipeptide residues has been regarded as a novel bio-nanostructure that can be applied to drug delivery systems, tissue-engineering scaffolds, batteries, capacitors and biosensors (Beker et al., 2010; Park and Kim, 2011; Ryu et al., 2010; Smith et al., 2008; Song et al., 2004).

In this study we synthesized PNTs and use them to encapsulate the enzymes which form a sensor matrix with potential for diabetic glucose diagnostics. When encapsulated inside a PNT it has been shown that the enzyme activity could be retained for an extended period of time even under unfavorable conditions for enzymes (Yu et al., 2005). The unique properties of PNT, such as excellent biocompatibility and electrical conductivity, provide enzymes with advantages of stable immobilization, protection from harsh environments, and superior signal transfer. Recently, it has been demonstrated that peptide nanostructures in biosensors can facilitate the detection of various compounds including hydrogen peroxide (Yemini et al., 2005a), NADH (Yuan et al., 2011), ethanol (Yemini et al., 2005b), phenolic compounds (Kim et al., 2011a), organophosphates (Kim et al., 2011b), Pb (Rica. et al., 2010) and Cu (Viguier et al., 2011).

For glucose detection, in general, glucose oxidase ($GO_x$) is used in glucose sensors. The detection mechanism is based on the electrochemical oxidation of hydrogen peroxide produced from the oxidation of glucose at a high potential with help of $GO_x$

* Corresponding author. Tel.: +1 419 530 8084; fax: +1 419 530 8086.
*E-mail address:* dong.kim@utoledo.edu (D.-S. Kim).

0956-5663/$ - see front matter © 2012 Elsevier B.V. All rights reserved.
http://dx.doi.org/10.1016/j.bios.2012.06.005

(Fu et al., 2011). However, at a high potential, various oxidative compounds, such as uric acid and ascorbic acid that are commonly present in biological samples may produce undesirable interfering reactions for the quantification of the glucose (Benedetto et al., 1996). One of the approaches to overcome this problem is to use a bi-enzyme system of $GO_x$ and horseradish peroxidase (HRP) (Ghindilis and Kurochkin, 1994). A combination of $GO_x$ and HRP has been mostly applied to design a biosensor system for glucose detection (Delvaux et al., 2005; Li et al., 2009; Manesh et al., 2010).

To enhance the enzyme activity and stability, one of the enzymes was encapsulated by PNTs. Encapsulating HRP by a PNT was proven to be successfully in our previous study (Park et al., 2010a, b). Also, the activity of encapsulated HRP was observed to be further retained in comparison with free enzymes in a solution (Park et al., 2012). Motivated by these observations, the combination of the PNT-encapsulated HRP and $GO_x$ was examined as the main part of an amperometric biosensor for diabetes. To the best of our knowledge, there has been no report on a glucose sensor using binary enzymes, one of which is encapsulated into the PNT. In addition, the gold nanoparticle (AuNP) modified electrode and a binary SAMs were used in this system to immobilize the PNT and $GO_x$ on the electrode. It was supposed to enhance the biosensor performance and the attachment of the PNT onto the surface of the gold electrode (Park et al., 2011a, b; Zheng et al., 2011). The measurement was performed in the presence of an electron mediator hydroquinone. The optimized conditions for analytical performance of the developed biosensor were studied. The stability and reproducibility of the sensor were also evaluated. The results obtained in this study indicated the validity of the biosensor incorporated with the PNT encapsulation.

## 2. Material and methods

### 2.1. Materials and reagents

HRP (E.C 1.11.1.7, 59 Umg-1, from Horseradish), $GO_x$ (E.C 1.1.3.4, 192 Umg-1, from Aspergillus niger), D-(+)-glucose, 3-mercaptopropionic acid (MPA), 1-tetradecanethiol (TDT), Gold(III) chloride trihydrate ($HAuCl_4$), *N*-hydroxysuccinimide (NHS), *N*-(3-dimethylaminopropyl)-N'-ethylcarbodiimide hydrodhloride (EDC) and Nafion (5 wt%) were purchased from Aldrich and Fluka (Sigma, USA) and used without further purification. Potassium hydroxide (KOH), potassium nitrate ($KNO_3$), potassium ferrocyanide ($K_4Fe(CN)_6$), potassium ferricyanide ($K_3Fe(CN)_6$), potassium chloride (KCl), hydrogen peroxide ($H_2O_2$), sulfuric acid ($H_2SO_4$), sodium phosphate monobasic ($H_2NaO_4P$) and sodium phosphate dibasic ($HNa_2O_4P$) were analytical grade from Fisher Scientific (Fisher, USA) and used without further purification. All solutions were prepared with water purified to $>18$ MW with a Barnstead Nanopure system (Barnstead Co., USA) filtered through a 200 mm filter paper.

### 2.2. Apparatus and measurements

Cyclic voltammetry (CV) and differential pulse voltammetry (DPV) were performed using a Gamry Reference 600 potentiostat (Gamry Instruments, USA) with Gamry PHE 200 and PV 220 physical electrochemistry software programs. A three-electrode system in a conventional glass-made cell was used for electrochemical measurements with a bare polycrystalline gold electrode of 3 mm diameter as a working electrode, a platinum wire as an auxiliary electrode, and a Ag|AgCl|KCl (saturated) electrode as a reference electrode. All the potential values reported are given with respect to this reference electrode. All measurements were made in a Gamry VistaShield Faraday cage (Gamry Instruments, USA).

Electrochemical impedance spectroscopy (EIS) measurements were carried out using a Gamry Reference 600 potentiostat in 5 mM $Fe(CN)_6^{3-}/Fe(CN)_6^{4-}$ solution with 0.1 M KCl as a supporting electrolyte. Impedance spectra were collected in the frequency range from 0.1 Hz to 100 kHz with a potential amplitude of 5 mV rms at 10 points per decade. EIS results were analyzed by fitting the experimental impedance data to electrical equivalent circuit models. Parameters of the electrical equivalent circuits were obtained by fitting the impedance function to the measured Bode and Nyquist plots with a complex nonlinear least square (CNLS) program built in the Gamry EIS 300 electrochemical impedance spectroscope.

The instrument used for characterization of the AuNP deposited on the bare gold electrode and the PNT modified electrode was field emission scanning electron microscopy (FE-SEM) (Hitachi S-4800, Japan). The electrodes were examined at 2 kV acceleration voltages.

### 2.3. Electrode preparation

#### 2.3.1. Encapsulation of the enzyme into a PNT

The PNT was prepared by dissolving a lyophilized form of the dipeptide of 1,1,1,3,3,3-hexafluoro-2-propanol at 100 mg $ml^{-1}$. The self-assembly of the PNT was carried out at the optimal concentration of 2 mg $ml^{-1}$. It was known that the concentration is a crucial factor for forming self-assembled PNTs (Reches and Gazit, 2003). To encapsulate HRP inside the PNT, first 1 ml of the PNT solution in a vial was placed in an oven at 35 °C to dry completely. Next, 1 ml of 50 mM phosphate buffer solution (PB, pH 7.0) containing HRP at the concentration of 1 mg $ml^{-1}$ was added into the vial that contained the dried PNT. It was then mixed using a vortex mixer subsequently. Finally, the enzyme-PNT solution was incubated in a shaker at 5 °C, 120 rpm for a week. It is thought that the HRP was encapsulated inside the hollow structure of the PNT due to the capillary effect (Yu et al., 2005; Yang et al. 2004) and stabilized on the inner surface of PNT (Park et al., 2010b).

In order to obtain the solution containing the HRP encapsulated into the PNT, the micro centrifugation was carried out at 16,000 g for 10 min. After separating the PNT from the solution, the PNT was thoroughly washed three times with the PB solution to remove the excess HRP (Park et al., 2010b).

#### 2.3.2. Gold nanoparticle modified electrode

Gold electrodes were mechanically polished with 0.5, 0.3, and 0.05 μm sizes of alumina suspensions on a polishing microcloth (Buehler, USA). Then they were sonicated in DI water and ethanol for 5 min. Polycrystalline gold electrodes were treated by piranha solution (a mixture with 3:1 of concentrated sulfuric acid and 30% hydrogen peroxide) for 15 min. Piranha solution is extremely reactive with organic materials and has to be used with sufficient protection. The pretreated clean gold electrodes were immersed in 0.1 M $KNO_3$ solution containing 3 mM $HAuCl_4$. Electrochemical deposition of gold nanoparticles (AuNP) on a planar gold electrode was carried out at the working potential of −200 mV vs. Ag|AgCl (sat'd KCl) for 330 s (Park et al., 2011a). Previously, it was confirmed that an increase in the surface area of the electrode could be performed by the deposition of 3D structural AuNP (Park et al., 2011b).

#### 2.3.3. Formation of a binary self-assembled monolayer onto the AuNP electrode

Thiol solution was prepared by mixing 1 mM ethanol solutions of MPA and TDT at a ratio of 9:1 while keeping the total concentration of the binary SAM at 1 mM (Park et al., 2011a, b). The binary SAM of MPA and TDT was formed on the AuNP electrode by soaking the electrodes into the mixed thiol solution for 1 h. The electrodes were subsequently rinsed in ethanol and DI water.

#### 2.3.4. Fabrication of AuNP-SAMs-PNT/HRP-$GO_x$ electrode

AuNP-SAMs modified electrode was immersed in a solution of 1 mM EDC and 3 mM NHS for 1 h to activate the terminal carboxylic acid groups of MPA. In this step, EDC converts the carboxyl group into a reactive intermediate, which is susceptible to attack by amines of the PNT. After the activation and rinsing the electrodes with the PB solution, a 10 μl of the PNT/HRP solution was immediately placed onto the electrode surface and then was allowed to dry at 4 °C. Then, a 10 μl of 3 mg $ml^{-1}$ $GO_x$ solution spread evenly onto the AuNP-SAMs-PNT/HRP electrode and was allowed to dry at 4 °C. Finally a 1 μl of 0.5 wt% Nafion solution was dropped on top of the AuNP-SAMs-PNT/HRP-$GO_x$ electrode. After drying, the electrode was immersed in the PB solution to wash away the non-immobilized residuals. All the modified electrodes were stored at 4 °C when not in use. The procedure for preparing glucose sensor is schematically shown in Fig. 1.

### 2.4. Real sample measurements

The sensor prepared in this work examined with human serum samples (Atlanta biologicals, USA). Each sample was diluted 10 times in the buffer solution. The diluted samples were then analyzed by the developed biosensor at a working potential of 0.03 V. The measured current was converted to the glucose concentration by using the calibration curve. The results were compared with those obtained YSI 2300 STAT plus glucose analyzer (YSI life sciences, USA).

The optimum response of the electrode in amperometric measurements was determined by measuring the current responses of 0.5 mM glucose in 50 mM PBS at pH values, 5.8, 6.4, 7, 7.7, 8.1.

## 3. Results and discussion

### 3.1. Characterization of the AuNP-SAMs-PNT/HRP-$GO_x$ electrode

The surface morphology of the gold electrodes was observed by FE-SEM. Fig. 1 shows the representative schematic for the modified electrodes and the SEM images of each layer. Fig. 1A and B show nanoscale images of the bare Au electrode and AuNP-SAMs modified electrode surfaces. It was found that gold nanoparticles were successfully formed on the surface of electrode, showing a relatively rough surface. Fig. 1C represents that the PNT/HRP was immobilized onto the AuNP-SAMs modified electrode surface. It is thought that the immobilization mechanism could be taken place not only through amine coupling (EDC/NHS chemistry) but also hydrophobic interaction between the PNT and the terminal methyl group of TDT.

### 3.2. Electrochemical behavior of the modified electrode

We used electrochemical impedance spectroscopy (EIS), cyclic voltammetry (CV) and differential pulse voltammetry (DPV) to characterize the electrochemical behavior of the modified electrode.

#### 3.2.1. Electrochemical impedance spectroscopy

EIS is an effective and non-destructive method for characterizing the interfacial electrical properties of modified surfaces of electrodes. This method can provide the information such as resistance and capacitance of an electrode.

Fig. 2 compares the Nyquist plots of the modified electrodes in $Fe(CN)_6^{3-}/Fe(CN)_6^{4-}$. The equivalent circuit (inset of Fig. 2A) is chosen to fit the impedance data. The AuNP modified gold electrode exhibits an almost straight line (Fig. 2A (curve a)) that is a very low $R_{et}$ of 90 Ω and that is characteristics of the diffusion limited electron-transfer process. After the binary SAM of MPA and TDT is deposited, the larger semicircle (Fig. 2A (curve b)) with an interfacial resistance of 759 Ω, due to the formation of the SAM layer on the electrode surface. Moreover, TDT, consisted of $-CH_3$ and SH, resulted in the hydrophobic surface area. Upon

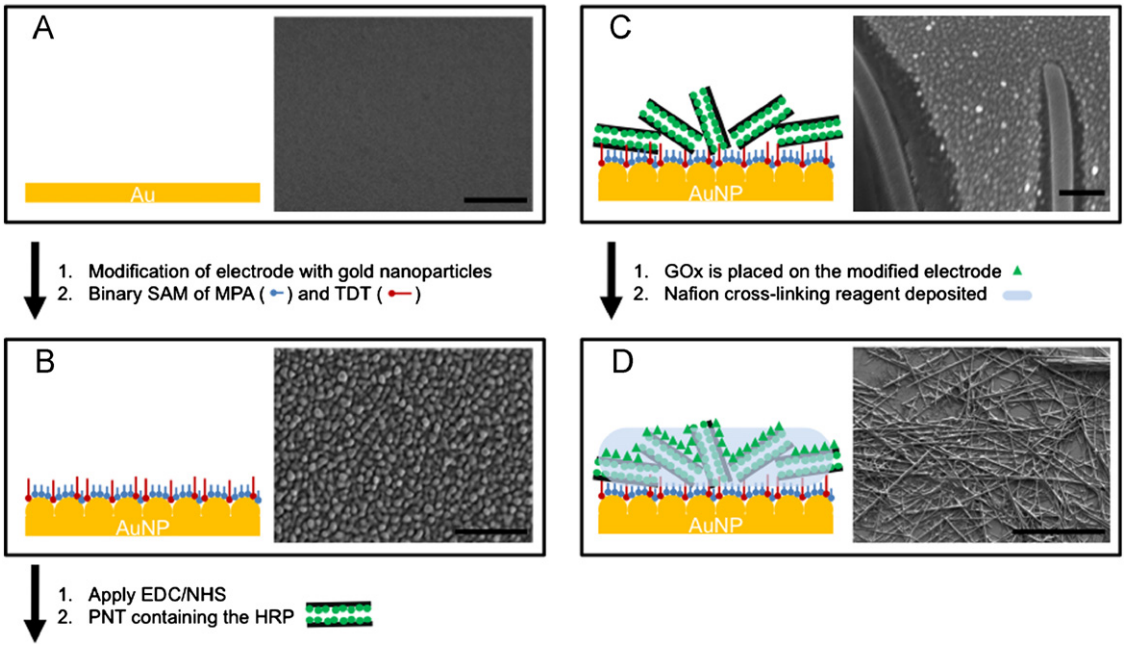


**Fig. 1.** The representative schematic for the modified electrode and the SEM images of each layer. SEM images of (A) Bare Au, (B) AuNP-SAMs, (C) AuNP-SAMs-PNT and (D) AuNP-SAMs-PNT-Nf. Scale bar = 500 nm (A), (B) and (C) and 300 μm (D).

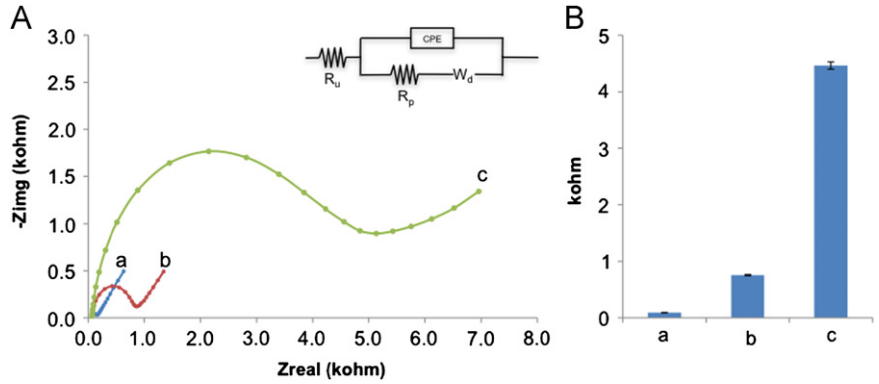


**Fig. 2.** Comparison of the Nyquist plots of the electrodes and the electron transfer resistance of the each layer. (A) Nyquist plots of impedance spectra obtained in the presence of 5 mM $Fe(CN)_6^{3-}/Fe(CN)_6^{4-}$ with 50 mM PB solution (pH 7.0) and 0.1 M KCl at (a) AuNP, (b) AuNP-SAMs and (c) AuNP-SAMs-PNT/HRP-$GO_x$ electrode. The frequency range from 0.1 Hz to 100 kHz with a potential amplitude of 5 mV rms at 10 points per decade. The inset shows the equivalent circuit applied to fit the data. (B) The values of electron transfer resistance ($R_{et}$) of the each layer.

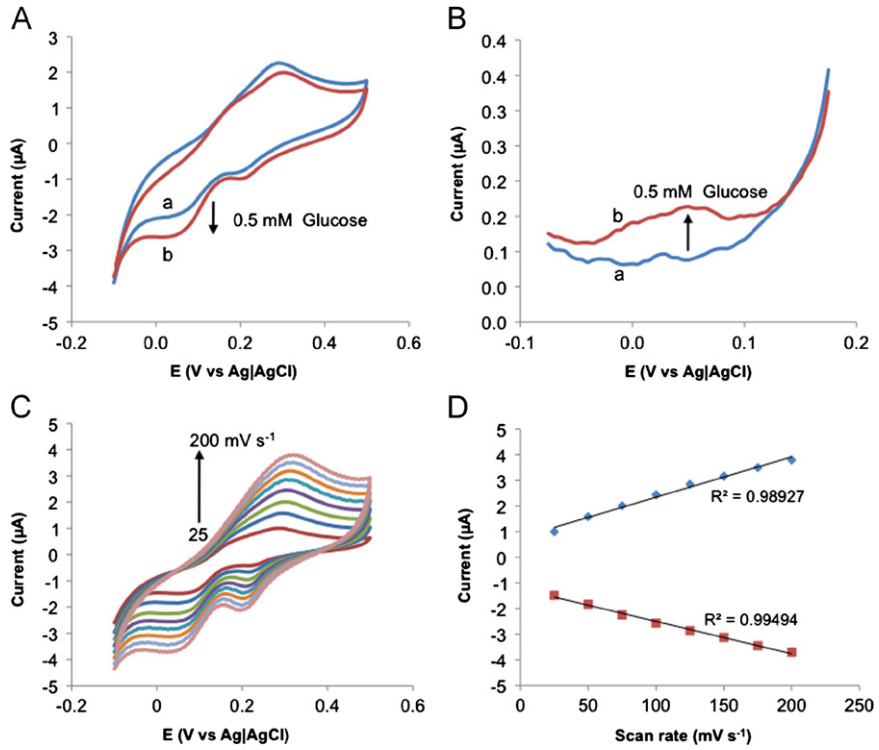


**Fig. 3.** Effects of glucose on the electrochemical response. (A) Cyclic voltammogram of AuNP-SAMs-PNT/HRP-$GO_x$ electrode (a) in the absence and (b) in the presence of 0.5 mM glucose. (B) Differential pulse voltammograms of the electrode (a) in the absence and (b) in the presence of 0.5 mM glucose. (C) Cyclic voltammograms of the electrode at different scan rates (25–200 mV $s^{-1}$). (D) Anodic and cathodic current plotted against the scan rate.

immobilization of PNT/HRP and $GO_x$ over the AuNP-SAMs modified electrode, the $R_{et}$ for the redox process of the probe drastically increased to 4464 Ω (Fig. 2A (curve c)). This is due to the attachment of the PNT and enzymes that increases the extent of insulation of the conductive support by the hydrophobic materials.

### 3.2.2. Voltammetry

Upon the addition of glucose, the AuNP-SAMs-PNT/HRP-$GO_x$ electrode triggers bioelectrocatalytic reaction, which changes the cyclic voltammogram with the cathodic current (Fig. 3A). The increase in the current is caused by the cascade of reactions taking place at the electrode surface. The DPV experiments have also been performed, which corresponded to the CV results. When the DPV was carried out, an obvious difference could be observed (Fig. 3B).

The enzymatic reaction mechanism of the AuNP-SAMs-PNT/HRP-$GO_x$ electrode developed here is described as follows:

$$\text{HRP (Red)} + H_2O_2 \rightarrow \text{HRP (Ox)} + 2H_2O$$

$$\text{HRP(Ox)} + \text{HQ} \rightarrow \text{HRP (Red)} + \text{BQ}$$

$$\text{BQ} + 2e^- + 2H^+ \rightarrow \text{HQ}$$

The substrate, glucose reacts with $GO_x$, in the presence of the natural co-substrate $O_2$, to generate hydrogen peroxide ($H_2O_2$). The $H_2O_2$ serves as substrate for HRP, resulting in the oxidized state of HRP which can be reduced by the redox mediator hydroquinone (HQ).

Moreover, the peak currents of the AuNP-SAMs-PNT/HRP-$GO_x$ electrode are shown to be dependent on the scan rate (Fig. 3C). The anodic and cathodic peak currents increase linearly with the scan rate, with correlation coefficients ($R^2$) values of 0.9893 and 0.9949 for the anodic and cathodic peaks, respectively, in the scan rate range of 25–200 mV $s^{-1}$. This linearity between peak current and scan rate shows that the redox reactions are surface-confined electrode reactions.

### 3.3. Effect of pH and operational potential effects on response of the bi-enzyme electrode

The pH of the buffer solution is essential to the sensitivity of biosensors. The pH affects the enzyme activity and the electrochemical behavior of $GO_x$. It was known that the range of the optimal pH for $GO_x$ is 6.5 − 7.5, which can vary with immobilization methods. The experimental results in the current study showed that the response signal increases with pH up until pH 7, and then it decreases at a higher pH range ($30 \pm 1.5$ nA at pH 5.8, $45 \pm 2$ nA at pH 6.4, $78 \pm 2.3$ nA at pH 7, $63 \pm 2$ nA at pH 7.7 and $41 \pm 1.3$ nA at pH 8.1). The low current response at the high and low pH ranges could possibly be raised by decreasing the enzyme activity. It turned out that the optimum pH for the biosensor developed would be pH 7. For further studies the PB solution with pH 7 was used as a working electrolyte for glucose detection.

### 3.4. Amperometric response to glucose

Amperometric measurements are widely used to evaluate the performance of enzyme-based sensors. Amperometric responses of the electrode were collected at a constantly applied potential of 0.03 V vs. Ag|AgCl electrode. Upon the each injection of 0.2 mM glucose in a range of 0.2–8.0 mM at regular intervals, the response shows a rapid and prominent increase in current, as shown in Fig. 4A. The biosensor response reaches 95% of a steady-state value within about 9–10 s at each glucose injection. The response time shows that there is no serious diffusion barrier through the hollow structure of the PNT. This response time is also comparable to that of 10 s for biosensor based on SBA-15 mesopores (Dai et al., 2008) and that of 8 s for carbon nanotube (CNT) biosensors (Zhu et al., 2007).

The corresponding calibration curve of the glucose sensor exhibits a linear response in the concentration range from 0.5 to 2.4 mM with a correlation coefficient of 0.994, which is compatible with that of 0.03–2.43 mM (Zhu et al., 2007). The detection limit was estimated to be 73.1 μM based on $3\sigma$ (where $\sigma$ is the standard deviation of the blank solution, number of experiments = 10), which is better than the reported value of 100 μM (Manesh et al., 2010). In the linear range, the slope (i.e., sensitivity) of 0.3 mA $M^{-1}$ was determined, which is higher than that of the reported value of 0.17 mA $M^{-1}$ (Benedetto et al., 1996; Manesh et al., 2010).

Fig. 4B also shows that the saturation of response current can be observed for the electrode in the calibration curve, which is consistent with the characteristic of the Michaelis–Menten kinetics. The apparent Michaelis–Menten constant ($K_m$), which is a reflection of the enzymatic affinity and an essential parameter to describe the enzyme-substrate kinetics of the biosensor, can be calculated from the electrochemical version of the Lineweaver–Burk plot (Fig. 4C) according to the following equation:

$$\frac{1}{I_{ss}} = \frac{1}{I_{max}} + \frac{K_m^{app}}{I_{max}}\left(\frac{1}{c}\right)$$

where $I_{ss}$ is the steady-state current after the addition of the substrate, $c$ is the bulk concentration of the substrate and $I_{max}$ is the maximum current measured under saturated substrate condition. The $K_m^{app}$ value was determined by the graphical analysis of the slope and intercept for the plot of the reciprocals of the steady

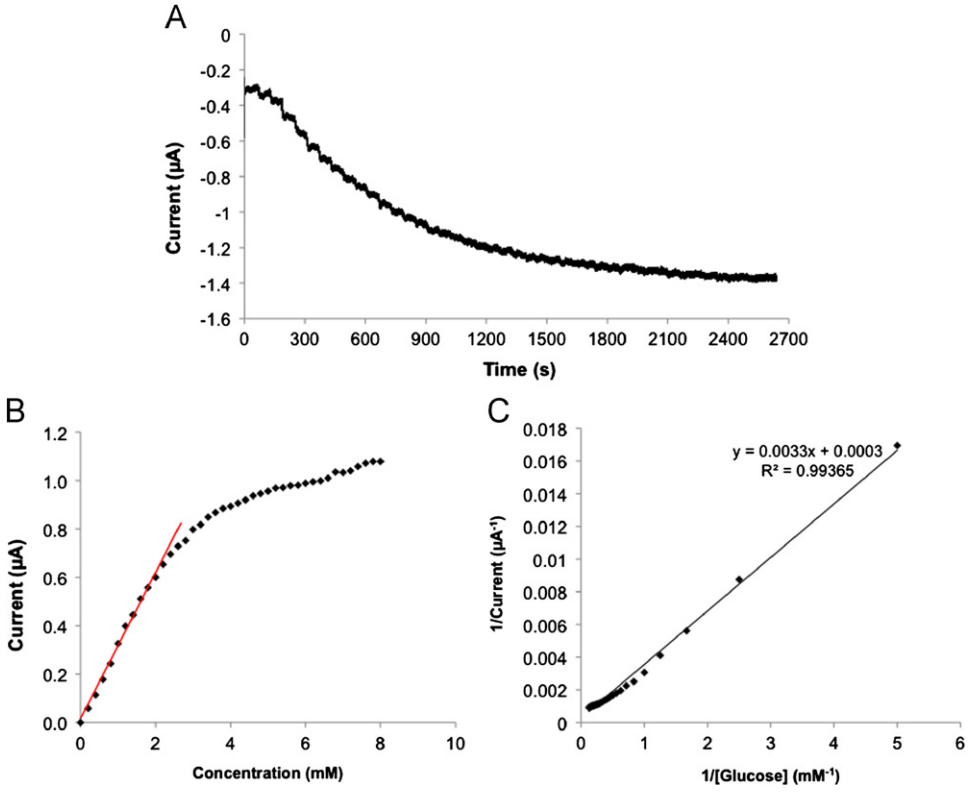


**Fig. 4.** Amperometric resonse of the electrode and its kinectics analyses. (A) Amperometric response of the AuNP-SAMs-PNT/HRP-$GO_x$ electrode upon successive addition of 0.2 mM glucose into 50 mM PB solution (pH 7.0) at 0.03 V. (B) Calibration curve of glucose sensor. (C) Lineweaver–Burk plot.

state current versus glucose concentration. The value of the $K_m^{app}$ was calculated 11 mM which suggested that the apparent affinity between the immobilized $GO_x$ and substrate be higher. This behavior of the sensor turns out to be governed by ideal Michaelis–Menten enzyme kinetics, which suggests that the enzymatic reaction rate constitute the rate-limiting step in the biosensor response. The observed $K_m^{app}$ value for the developed biosensor is lower than that in other previously reported bi-enzyme glucose sensor (49 mM) based on the use of poly(toluidine blue O) film. In this report, toluidine blue O was applied as a mediator and polymerized on multi-walled carbon nanotube (MWNT) modified glassy carbon electrode to improve the performance of the biosensor (Wang et al., 2010). The lower value implies the strong affinity of substrate to the enzymes, resulting in a facilitated enzymatic reaction. It may be noted that the $K_m^{app}$ value depends on the nature of the immobilization matrix and the immobilization method.

### 3.5. Selectivity and interferences

The real sample for glucose detection contains other sugars and common species that could potentially interfere with the glucose detection. The interferences selected for the test are ascorbic acid (AS), sucrose (SU), galactose (GA), and lactose (LA). In light of low concentrations of these sugars in the blood, the interference needs to be seriously considered because their molecular structures are similar to that of glucose. Furthermore, because ascorbic acid could be easily oxidized at a relatively high overpotential, a lower working potential helps avoid the electrochemical reaction of the interferences. As shown in Fig. 5A., the current responses to 0.5 mM of AS, SU, GA and LA are negligible compared to 0.2 and 0.5 mM of glucose. The results are due to the excellent selectivity of the AuNP-SAMs-PNT/HRP-$GO_x$ electrode and the lower working potential. Moreover, the Nafion acting as an effective permselective layer could eliminate the interferences and increase the selectivity of the developed biosensor.

### 3.6. Reproducibility and stability

The precision of the developed bio-sensing system was characterized in terms of repeatability and reproducibility. For the repeatability, successive amperometric measurements with the same electrode were carried out. Sets of eight successive calibrations for 0.5 mM glucose were constructed yielding a relative standard deviation (RSD) of 1.95% for their slopes. Furthermore, the reproducibility of the sensor measurements was investigated. The RSD for three different electrodes using the same conditions was 5.74% corresponding to 0.5 mM glucose. These results show that the fabrication procedure of the biosensor is reliable and that the modified electrodes are reproducible.

Long-term stability is a basic requirement for the development of biosensors. The stability of the AuNP-SAMs-PNT/HRP-$GO_x$ electrode was evaluated and its response to 0.5 mM of glucose was measured for one month. The electrode, when not in use, was stored in the PB solution at 4 °C. The results in Fig. 5.B showed that 85% of the initial response remained after a storage of one month. The decrease in the current response may be due to a loss of the enzyme activity in long-time keeping. However, the excellent performance of the sensor after one month storage could be attributed to the following aspects: Good long-term stability of this sensor system can be attributed to the excellent biocompatibility of the PNT for retaining the enzyme activity. Also, it is possibly that the hollow structure of the PNT provides mild environment around the enzymes. Table 1 shows the

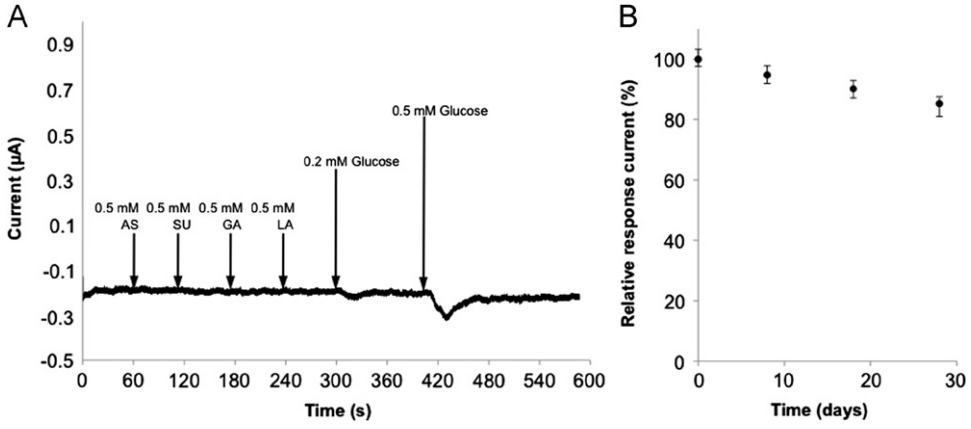


**Fig. 5.** Stability analyses of the electrode. (A) Influence of electroactive interferences of ascorbic acid (AS, 0.5 mM), sucrose (SU, 0.5 mM), galactose (GA, 0.5 mM) and lactose (LA, 0.5 mM). The working potential=0.03 V. (B) Long-term stability of the AuNP-SAMs-PNT/HRP-GO*x* electrode stored in the PB solution (pH 7.0) at 4°C.

**Table 1**
Comparison of the performance of various bienzymatic glucose biosensors.

| Components of biosensor | Sensitivity ($mA\ M^{-1}$) | Stability (days/percent of the initial response) | References |
|---|---|---|---|
| AuNP-SAMs-PNT/HRP-$GO_x$ | 0.3 | 30/85 | Current work |
| ITO/PTMSPA/HRP-$GO_x$ | 0.16 | 50/55 | Manesh et al. (2010) |
| GC/CNT/HRP-$GO_x$/PTBO | 113 | 25/75 | Wang et al. (2010) |
| Au/CS/Con A/HRP-$GO_x$ | 1.18 | 35/89 | Li et al. (2009) |
| GC/SBA-15/HRP-$GO_x$ | 90 | 60/60 | Dai et al. (2008) |
| Au/SWNT/HRP-$GO_x$/PPy | 1.03 | 14/67 | Zhu et al. (2007) |
| PC/Au/MPE/GA/HRP/GA/$GO_x$ | 400 | – | Delvaux et al. (2005) |
| GC/HRP-$GO_x$/PPy | 0.17 | 4/75 | Benedetto et al. (1996) |
| GE/CB/HRP-$GO_x$ | – | 40/50 | Ghindilis and Kurochkin (1994) |

**Table 2**
Determination of glucose concentration contained in human serum samples.

| Sample no. | Determined by biosensor[a] (mM) | Given by glucose analyzer[b] (mM) | Relative deviation (%) |
|---|---|---|---|
| 1 | $0.546 \pm 0.051$ | 0.504 | 7.69 |
| 2 | $0.368 \pm 0.012$ | 0.370 | 0.54 |
| 3 | $0.618 \pm 0.069$ | 0.594 | 3.88 |

[a] Mean $\pm$ S.D. of three measurements.
[b] Value obtained by the commercial glucose analyzer.

characteristics of AuNP-SAMs-PNT/HRP-$GO_x$ in terms of sensitivity and stability are compared with earlier reported bi-enzymatic glucose biosensors.

### 3.7. Real sample analysis

The practical usage of the developed glucose biosensor was carried out with human serum samples. A series of human serum samples were analyzed. The sample was 10-fold diluted with 50 mM PB at pH 7. The diluted samples were then analyzed by the developed biosensor at a working potential of 0.03 V. The measured current was converted to the glucose concentration by using the calibration curve. The results were compared with those obtained YSI 2300 STAT plus glucose analyzer (YSI life sciences, USA). In Table 2, the values obtained from our biosensor system are close to those from the analyzer. It can be concluded that the values from the glucose sensor developed are in good agreement with those from the commercial instrument for the glucose detection, demonstrating that the developed sensor has a great potential for the practical usage for real clinical samples.

## 4. Conclusions

The results demonstrate the possible use of the PNT to conveniently fabricate a new bi-enzyme glucose biosensor. The encapsulation of HRP inside the PNT was shown to provide a spatially biocompatible environment on the electrode surface, which could further retain the enzyme activity for an extended period of time. Moreover, the spatially aligned aromatic compounds were considered to enhance the electron transfer. Therefore, the developed glucose sensor appears to exhibit reasonable sensitivity, reproducibility and long-term stability. The methodology applied in this study possibly provides a new platform for the fabrication of biocompatible glucose sensor and other types of biosensors.

## Acknowledgments

The CMSC (Center for materials and sensor characterization) at University of Toledo is acknowledged for the use of instruments. Financial support from Nano-STAR Center at Kwangwoon University, and Kwangwoon University (2011) is gratefully acknowledged.

## References

Adler-Abramovich, L., Badihi-Mossberg, M., Gazit, E., Rishpon, J., 2010. Small 6, 825–831.
Beker, P., Koren, I., Amdursky, N., Gazit, E., Rosenman, G., 2010. Journal of Materials Science 45, 6374–6378.
Benedetto, G.E.D., Palmisano, F., Zambonin, P.G., 1996. Biosensors and Bioelectronics 11, 1001–1008.
Dai, Z., Bao, J., Yang, X., Ju, H., 2008. Biosensors and Bioelectronics 23, 1070–1076.
Delvaux, M., Walcarius, A., Demoustier-Champagne, S., 2005. Biosensors and Bioelectronics 20, 1587–1594.
Fu, G., Yue, X., Dai, Z., 2011. Biosensors and Bioelectronics 26, 3973–3976.
Gazit, E., 2007. Chemical Society Reviews 36, 1263–1269.
Ghindilis, A.L., Kurochkin, I.N., 1994. Biosensors and Bioelectronics 9, 353–357.
Kim, J.H., Lim, S.Y., Nam, D.H., Ryu, J., Ku, S.H., Park, C.B., 2011a. Biosensors and Bioelectronics 26, 1860–1865.
Kim, J.H., Ryu, J., Park, C.B., 2011b. Small 7, 718–722.
Li, F., Wang, Z., Chen, W., Zhang, S., 2009. Biosensors and Bioelectronics 24, 3030–3035.
Manesh, K.M., Santhosh, P., Uthayakumar, S., Gopalan, A.I., Lee, K.P., 2010. Biosensors and Bioelectronics 25, 1579–1586.
Park, B.W., Kim, D.S., 2011. Peptide nanotubes in biomedical and environmental applications. In: Mukhopadhyay, S.M. (Ed.), Nanoscale Multifunctional Materials: Science and Applications, 1st ed. John Wiley & Sons, Inc., New Jersey, pp. 369–391.
Park, B.W., Yoon, D.Y., Kim, D.S., 2010a. Biosensors and Bioelectronics 26, 1–10.
Park, B.W., Yoon, D.Y., Kim, D.S., 2010b. ECS Transactions 33, 25–29.
Park, B.W., Kim, D.S., Yoon, D.Y., 2011a. Korean Journal of Chemical Engineering 28, 64–70.
Park, B.W., Yoon, D.Y., Kim, D.S., 2011b. Journal of Electroanalytical Chemistry 661, 329–335.
Park, B.W., Ko, K.A., Yoon, D.Y., Kim, D.S., 2012. Enzyme and Microbial Technology 51, 81–85.
Reches, M., Gazit, E., 2003. Science 300, 625–627.
Reches, M., Gazit, E., 2006. Nature Nanotechnology 1, 195–200.
Rica., R., Mendoza, E., Matsui, H., 2010. Small 6, 1753–1756.
Ryu, J., Kim, S.W., Kang, K., Park, C.B., 2010. Advanced Materials 22, 5537–5541.
Smith, A.M., Williams, R.J., Tang, W., Coppo, P., Collins, R.F., Tuner, M.L., Saiani, A., Ulijn, R.V., 2008. Advanced Materials 20, 37–41.
Song, Y., Challa, S.R., Medforth, C.J., Qiu, Y., Watt, R.K., Pena, D., Miller, J.E., Swol, F.V., Shelnutt, J.A., 2004. Chemical Communications 9, 1044–1045.
Viguier, B., Zor, K., Kasotakis, E., Mitraki, A., Clausen, C.H., Svendsen, W.E., Castillo-Leon, J., 2011. ACS Applied Materials & Interfaces 3, 1594–1600.
Wang, W., Wang, F., Yao, Y., Hu, S., Shiu, K.K., 2010. Electrochimica Acta 55, 7055–7060.
Yan, X., Zhu, P., Li, J., 2010. Chemical Society Reviews 39, 1877–1890.
Yang, B., Kamiya, S., Shimizu, Y., Koshizaki, N., Shimizu, T., 2004. Chemistry of Matterials 16, 2826–2831.
Yemini, M., Reches, M., Gazit, E., Rishpon, J., 2005a. Analytical Chemistry 77, 5155–5159.
Yemini, M., Reches, M., Rishpon, J., Gazit, E., 2005b. Nano Letters 5, 183–186.
Yu, L., Banerjee, I.A., Gao, X., Nuraje, N., Matsui, H., 2005. Bioconjugate Chemistry 16, 1484–1487.
Yuan, J., Chen, J., Wu, X., Fang, K., Niu, L., 2011. Journal of Electroanalytical Chemistry 656, 120–124.
Zheng, R., Park, B.W., Kim, D.S., Cameron, B.D., 2011. Biomedical Optics Express 2, 2731–2740.
Zhu, L., Yang, R., Zhai, J., Tian, C., 2007. Biosensors and Bioelectronics 23, 528–535.